

Revealing the Intrinsic Uneven Electrochemical Reactions of Li Metal Anode in Ah-Level Laminated Pouch Cells

Xiangrui Duan, Lingyue Wang, Guocheng Li, Xueting Liu, Mintao Wan, Junmou Du, Renming Zhan, Wenyu Wang, Yuanjian Li, Shuibin Tu, Yue Shen, Zhi Wei Seh, Li Wang, and Yongming Sun*

The uneven electrochemical reactions of lithium (Li) metal anode is one of the main reasons that hinder its application in rechargeable high energy density batteries. Great progress has been achieved in homogenizing electrochemical reactions of Li metal anode in lab-scale coin cells, however, it cannot be directly applied to pouch cells, where undesirable defects or side reactions are significantly aggravated. With carbonate electrolyte, multi-layered negative and positive electrodes (8 × 11 cm), 1.2 Ah sulfurized polyacrylonitrile (SPAN)||Li pouch cell lost all its capacity after 40 cycles under a current of 600 mA, although its counterpart with coin cell configuration showed much higher capacity retention of 94% under the same test condition. Severe corrosion with uneven, porous, dendritic Li deposits is observed for pristine Li electrode in a pouch cell, especially in the near-tab and the central regions with close connection with the current collector due to the locally amplified current densities. In contrast, Li/Li–Sn alloy composite electrode displays uniform and dense Li plating behavior over the entire test area with significantly suppressed parasitic reactions and gas evolution. As such, a 1.2 Ah SPAN||Li/Li–Sn cell displays much higher capacity retention than SPAN||Li cell (87% for 100 cycles vs. 0 for 40 cycles).

1. Introduction

The development of high energy density battery technologies beyond Li-ion chemistry is of vital importance to meet the ever-increasing energy demand of electric vehicles and grid energy storage.^[1] Rechargeable Li metal batteries are regarded as one of the most promising high energy density battery technologies employing Li metal as the anode, since Li metal delivers the highest theoretical specific capacity (3860 mA h g⁻¹) and lowest reduction potential (−3.04 V vs. standard hydrogen electrode) among the existing Li-based chemistries.^[2] Nevertheless, the practical application of Li metal anode is hindered by several significant challenges, including uneven electrochemical reactions and high reactivity of Li metal electrode.^[3] Till now, intensive efforts have been devoted to stabilizing Li electrodes, such as electrolyte optimization (e.g., high/localized-high concentration electrolyte^[4] and dual-salt electrolyte^[5]), interface engineering (e.g., inorganic carbon

coating^[6] and self-assembled monolayers interface^[7]), and electrode structure design (e.g., three-dimension Li/graphene composite^[8] and Li in ion-conductive host^[9]). Among these strategies, composite Li metal anode design provides rich active sites and a stable framework for Li metal, achieving significant success in homogenizing Li plating/stripping electrochemical reactions and prolonging battery lifespan.^[10] However, most of these studies are carried out based on laboratory-scale coin cells or single-layer pouch cells, whose experimental parameters and working environments are far from practical batteries, such as Ah-level laminated pouch cells, and thus cannot provide direct guidance for their improvement.^[11]

To realize practical Li metal batteries, electrodes should possess high mass loading, high density, low electrolyte/capacity (E/C) ratio, and low negative/positive capacity (N/P) ratio,^[12] which are rarely discussed in studies using coin cell or single-layer pouch cell configurations. Also, the working environments for practical Ah-level laminated pouch cells are significantly different from that for coin cells, arising from electrode structure, total current, and pressure. **Figure 1** shows the schematics of a coin cell and a laminated pouch cell with large

X. Duan, L. Wang, G. Li, M. Wan, J. Du, R. Zhan, W. Wang, Y. Li, S. Tu, Y. Sun

Wuhan National Laboratory for Optoelectronics
Huazhong University of Science and Technology
Wuhan 430074, China
E-mail: yongmingsun@hust.edu.cn

X. Liu, S. Tu, Y. Shen
School of Materials Science and Engineering
Huazhong University of Science and Technology
Wuhan 430074, China

Z. W. Seh
Institute of Materials Research and Engineering
Agency for Science
Technology and Research (A*STAR)
2 Fusionopolis Way, Innovis, Singapore 138634, Singapore

L. Wang
Institute of Nuclear & New Energy Technology
Tsinghua University
Beijing 100084, China

 The ORCID identification number(s) for the author(s) of this article can be found under <https://doi.org/10.1002/adfm.202210669>.

DOI: 10.1002/adfm.202210669

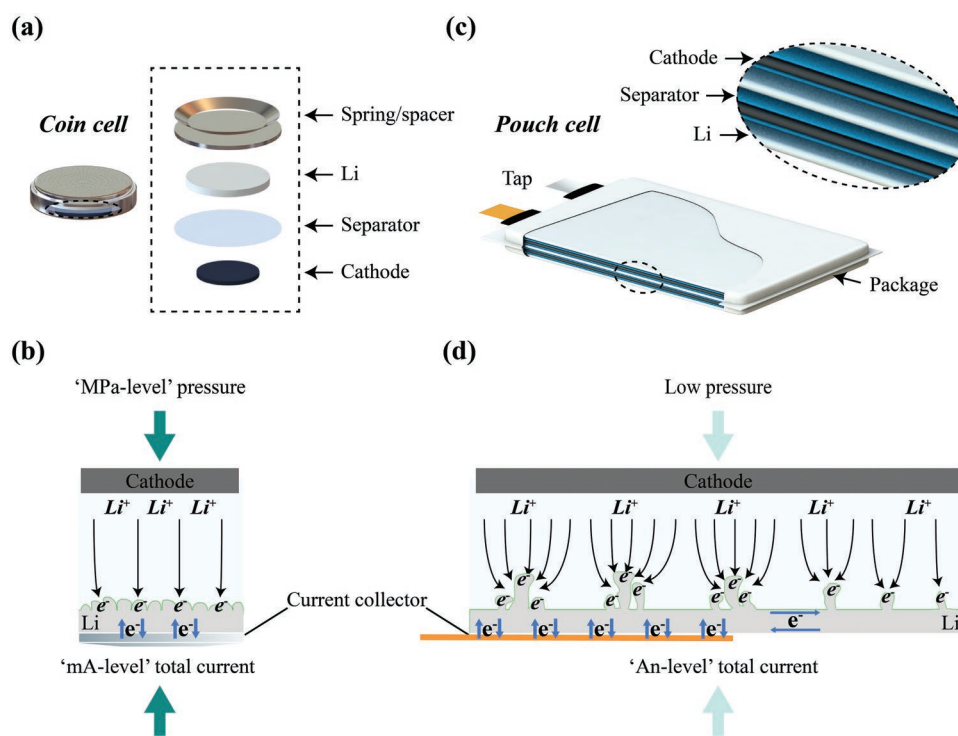


Figure 1. Comparison of coin cell and pouch cell configurations. a,b) Schematic illustration of coin cell and Li anode with mA-level total current, MPa-level pressure, and a spring/spacer component that covers the entire metallic Li electrode and serves as a current collector and pressurizer, enabling relatively uniform electrochemical reactions. c,d) Schematic illustration of pouch cell and Li anode with An-level total current and low pressure, where Cu foil current collector partially connects with the metallic Li anode (the near-tap and the central regions), leading to uneven electrochemical reactions.

structural differences. The coin cell possesses a spring/spacer, covering the entire Li metal electrode and serving as a current collector and pressurizer, while the pouch cell uses a Cu foil to conduct electrons, where only partial Li metal electrode contacts with it to avoid the introduction of excess inert materials and to elevate the energy density. Electron exchange between the external circuit and Li metal electrode is focused on the area covered by the Cu foil in laminated pouch cells compared to the whole electrode in coin cells. A large fraction of total current tends to distribute around the current collector region (including the near-tap and the central regions), leading to an interregional heterogeneity of the electrochemical reactions over a large-scale electrode, which becomes an important factor that causes the uneven electrochemical reactions over the entire electrode in pouch cells. In an Ah-level laminated pouch cell, the applied total current (ampere level) is often three orders of magnitude higher than that of a coin cell (milliamper level) during the charge/discharge processes.^[13] With the above differences, any minor defects inside practical pouch cells would be sharply magnified by locally huge current, which aggravates the overall uneven electrochemical reactions and causes rapid battery degradation. Moreover, there exists a huge difference in pressure between the two cell configurations. The electrodes sustain MPa-level pressure in coin cell configuration.^[14] Such high external pressure is beneficial to densifying lithium plating process by tuning the energy barrier and regulating the growth direction.^[15] Besides, huge pressure helps to maintain a percolation pathway for charges during Li stripping process,^[16]

extending the cycle life of Li metal anode. In Ah-level laminated pouch cells with the low/negligible pressure in comparison to coin cells, Li metal grows randomly into loose deposits and even dendritic structures, and the fast accumulation of electrochemically isolated metallic Li takes place during the Li stripping/plating cycling. Although Li metal electrodes in coin cell configuration could cycle over 1000 cycles,^[17] their reported cycle lives in Ah-level laminated pouch cell configuration were significantly reduced (e.g., <40 cycles).^[7,18] Therefore, intensive efforts should be devoted to understanding and addressing the uneven electrochemical reactions over large-scale electrodes in practical Li metal batteries and extending their cycle life.

In this contribution, we investigated the electrochemical Li plating/stripping behavior of pristine Li metal electrode and Li metal/lithium-tin alloy (Li/Li-Sn) composite electrode with fast lithium transport capability at different regions of large-scale electrodes in Ah-level laminated pouch cells, including the near-tap region, the central and the edge regions, and revealed the effect of different cell structures/electrode regions. Porous and dendritic Li deposits with loose structure was observed in pristine Li metal electrode with a size of 8 × 11 cm after cycling, where the near-tap and the central regions with close connection with the current collector showed more severe corrosion than the edge region due to the locally amplified current density, although cracks still spread over the entire edge region. In sharp contrast, uniform Li deposits with a dense structure were observed over different regions of a Li/Li-Sn

alloy composite anode, as well as suppressed parasitic reactions and gas evolution, supporting the positive effect of Li alloy composite anode design in homogenizing electrochemical reactions, and prolonging the lifespan in Ah-level laminated pouch cell configuration. As a demonstration, a 1.2 Ah SPAN||Li/Li-Sn pouch cell exhibited steady charge/discharge performance over 100 cycles with a capacity retention of 87% at 600 mA (1 C = 1200 mA, a cathode areal capacity of 3.4 mA h cm⁻²), far outperforming the 1.2 Ah SPAN||Li pouch cell that lost all its capacity after 40 cycles. This work first reveals the amplified inhomogeneity in electrochemical Li plating/stripping reactions caused by the difference in electrochemical environment for large-scale Li metal electrode in Ah-level laminated pouch cell under practical harsh test conditions, and the advancement of Li/Li-Sn alloy composite anode in eliminating the effect of uneven electrochemical reactions and suppressing side reactions.

2. Results and Discussion

To compare the electrochemical performance of Li/Li-Sn alloy composite and pristine Li anodes, coin and pouch cells were first assembled by pairing with a SPAN cathode (mass loading of 4.86 mg cm⁻²), which has been intensively investigated due to the high capacity, good cycling stability, and cost-effectiveness of sulfur.^[19] The SPAN||Li/Li-Sn coin cells offered a high reversible areal capacity of 3.14 mA h cm⁻² (specific capacity of 646 mA h g⁻¹) at 1 C (1 C = 700 mA g⁻¹) for the initial cycle, corresponding to a N/P ratio of 5, and 2.9 mA h cm⁻² (596 mA h g⁻¹) for the 150th cycle, delivering high capacity retention of 92% (Figure 2a; Figure S2b, Supporting Information). In sharp contrast, the capacity of SPAN||Li coin cells rapidly decayed from 3.15 mA h cm⁻² (647 mA h g⁻¹) to 1.48 mA h cm⁻² (304 mA h g⁻¹) after 150 cycles, showing much lower capacity retention of 47% under the same test condition (Figure 2b; Figure S2a,

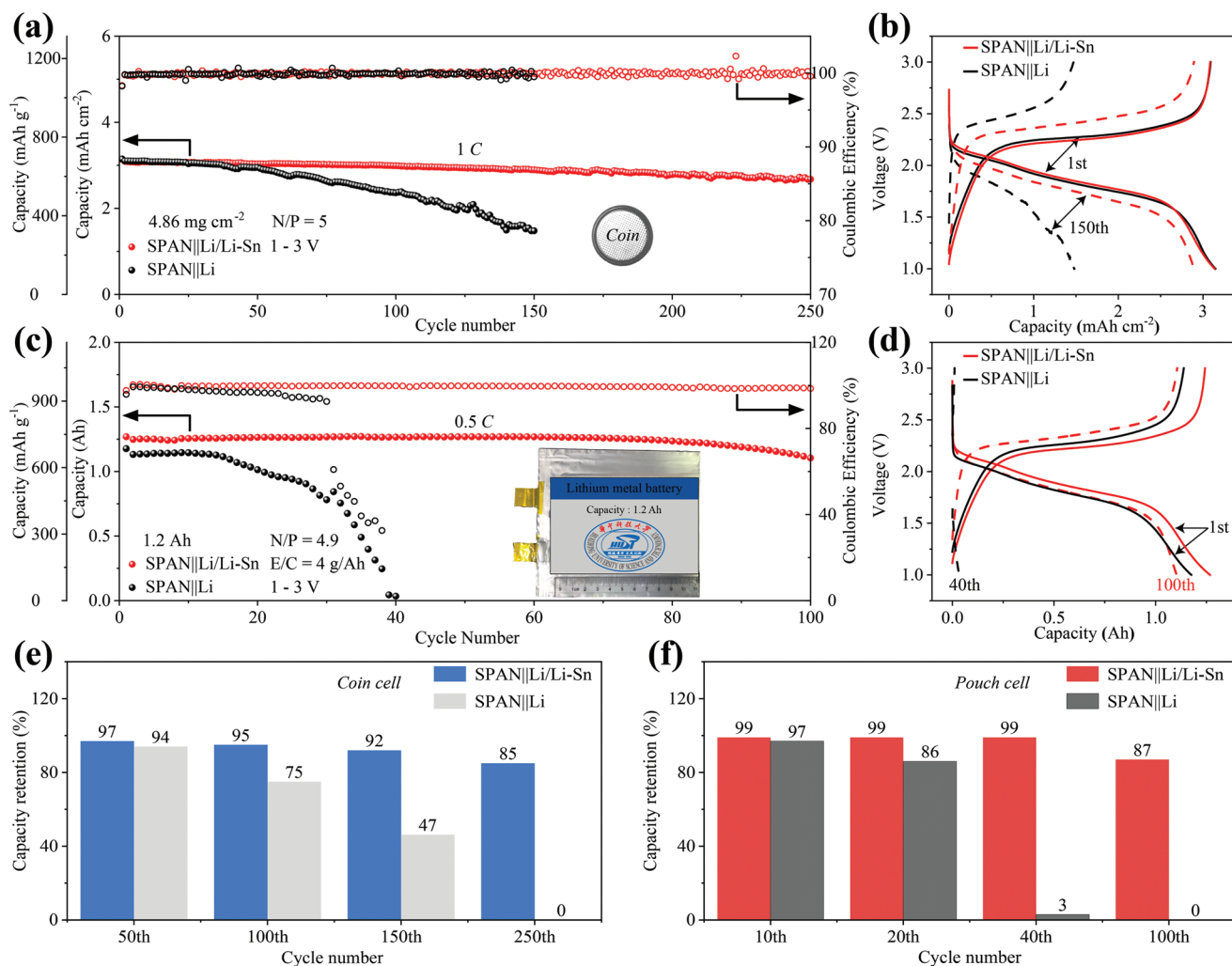


Figure 2. a) Electrochemical performance of SPAN||Li and SPAN||Li/Li-Sn coin cells at 1 C. The inset is a photograph of the as-prepared coin cell. b) Voltage profiles of SPAN||Li and SPAN||Li/Li-Sn coin cells for selected cycles in Figure 2a. c) Electrochemical performance of 1.2 Ah SPAN||Li and SPAN||Li/Li-Sn laminated pouch cells at 600 mA. The inset is a photograph of the as-prepared 1.2 Ah pouch cell. d) Voltage profiles of 1.2 Ah SPAN||Li and SPAN||Li/Li-Sn laminated pouch cells for selected cycles in Figure 2c. e) Comparison of capacity retention for SPAN||Li and SPAN||Li/Li-Sn coin cells for selected cycles in Figure 2a. f) Comparison of capacity retention for 1.2 Ah SPAN||Li and SPAN||Li/Li-Sn laminated pouch cells for selected cycles in Figure 2c.

Supporting Information). These cycling results, together with the result of rate capability measurement (Figure S3, Supporting Information), suggested prominent electrochemical performance of the Li/Li–Sn alloy composite anodes. Herein, we highlight the advancement of the Li/Li–Sn composite anode in Ah-level Li metal laminated pouch cells (N/P ratio of 4.9, E/C ratio of 4 g Ah⁻¹) (Figure 2c). Cycled at 600 mA, the SPAN||Li pouch cells showed an initial reversible capacity of 1.2 Ah and it decayed dramatically to 0.03 Ah after 40 cycles, showing low capacity retention of 3% (Figure S4a, Supporting Information). Impressively, the SPAN||Li/Li–Sn pouch cells exhibited a higher initial reversible capacity of 1.27 Ah and stable cycling with high capacity retention of 87% (1.1 Ah) for over 100 cycles (Figure 2d; Figure S4b, Supporting Information). The electrochemical results of Li/Li–Sn alloy composite and pristine Li electrodes in both coin and Ah-level laminated pouch cells suggested the significant role of composite anode design in stabilizing the Li metal anode and extending the cycle life (Figure 2e,f). It should be noted that the electrochemical results in Ah-level laminated Li metal pouch cells were much worse than that in coin cells, indicating that the operation of practical Li metal pouch cells is more challenging than that of coin cells. In consideration of the practical applications, the performance in coin cell configuration should be further verified using more practical cell configuration to validate the advancement of electrode design, electrolyte engineering, and others.

To reveal the effect of electrode structure on electrochemical Li plating/stripping behavior, and the mechanism of enhanced electrochemical performance of Ah-level laminated pouch cells using Li/Li–Sn alloy composite anode, the pristine Li and Li/Li–Sn composite anodes were characterized over different regions of the electrodes after 40 cycles, including the near-top region (RT), the central (RC), and the edge regions (RE) (Figure 3a). Optical images show different electrode states for the pristine Li electrode at the RT, RC, and RE regions. Materials peeling off was observed for the RT and RC regions (Figure 3b). The significant difference in local current density would cause uneven electric field at different regions of the electrode, and consequently different Li plating/stripping behavior. The electron aggregation effect at the RT and RC regions would lead to the amplified intensity in electric field in comparison to RE region, accounting for uneven electrochemical reactions and preferential corrosion in those regions. In contrast, the structure of the Li/Li–Sn anode remained intact over the tested three regions after 40 cycles (Figure 3b), suggesting the significant role of composite Li metal anode design in eliminating the negative effect of inhomogeneous electrochemical reactions and enhancing the structural stability of the anode. To further reveal the effect on electrochemical reactions caused by structural difference, the cycled electrodes were further studied using SEM. The cycled pristine Li electrode displayed obvious region-dependent electrode structures. The RT and RC regions displayed a highly porous geometry morphology with large cracks and vacancies (Figure 3c,d), suggesting deteriorative heterogeneous Li deposition. High-resolution SEM images revealed that the deposits consisted of loosely stacked Li dendrites with high porosity in RT and RC regions (Figures S5 and S6, Supporting Information), accounting for the abundant large cracks with a length of ≈500 μm. The RE

region of the cycled pristine Li electrode exhibited a relatively intact structure with fewer and smaller cracks, although they also spread over the entire tested region (Figure 3e). The difference in cycled electrode structures for the RT, RC, and RE regions arose from their different local electrochemical environments, which were caused by the uneven current distribution over large-scale electrodes in laminated pouch cells, and would not be shown/detected in coin cells. It can be inferred that such non-uniform electrochemical behavior could be further aggravated in electrodes with larger sizes and harsher test conditions. Interestingly, the Li/Li–Sn alloy composite electrode maintained a smooth surface and dense, integrated structure (Figure 3f–h), revealing its improved Li plating/stripping behavior over the entire tested electrode (8 × 11 cm). Similarly, uniform and smooth Li stripping morphology was observed for the Li/Li–Sn composite electrode after 40 Li stripping/plating cycles in comparison to the uneven surface with large and deep cavities for pristine Li electrode (Figure S7, Supporting Information). The above investigation demonstrated the significant role of Li alloy composite anode design in eliminating the negative effect of inhomogeneous electrochemical reactions that different electrode structures/regions cause. For example, the morphology and structure of Li deposits in all the tested regions were similar, although the local current density in RE region was lower than other regions. The explanation can be the Li plating behavior within the interior of the electrode and the fast lithium transport capability due to the Li–Sn alloy network of the Li/Li–Sn alloy composite electrode, which will be investigated in detail later.^[10] Although the Ah-level laminated pouch cell employing pristine Li anode almost lost all its capacity after 40 cycles (with 3% capacity retention), no significant capacity decay was observed for that with Li/Li–Sn alloy composite anode under the same test conditions (Figure 2c,f).

Linear sweep voltammetry (LSV) and temperature-dependent EIS measurements were further carried out to evaluate the Li⁺ transport property of the electrode. The exchange current densities (j_0) were calculated according to the LSV results. As illustrated in Figure 3i, the value of j_0 for the Li/Li–Sn alloy composite electrode was 0.72 mA cm⁻², which was one order of magnitude higher than that of 0.04 mA cm⁻² for the fresh pristine Li electrode, indicating much faster Li⁺ transport property at the electrolyte/electrode interface,^[20] which benefits from the Li–Sn alloy skeleton in the Li/Li–Sn alloy composite anode. Besides, the apparent activation energy (E_a), representing the energy barrier for Li⁺ transfer through solid electrolyte interphase (SEI) layer for fresh pristine Li and Li/Li–Sn alloy composite anodes,^[21] was calculated according to the results of temperature-dependent EIS measurement for Li||Li and Li/Li–Sn||Li/Li–Sn cells (Figure S8a,b and Tables S1 and S2, Supporting Information). The EIS curves from 263 to 288 K were analyzed to obtain the value of each impedance component by establishing an appropriate equivalent circuit (Figure S8c, Supporting Information). As shown in Figure 3j, the value of E_a for the Li/Li–Sn alloy composite anode (44.89 kJ mol⁻¹) was much lower than that of the fresh pristine Li anode (71.00 kJ mol⁻¹). The significantly reduced value of E_a in the Li/Li–Sn alloy composite electrode again verified that Li⁺ diffusion through the SEI was accelerated due to the

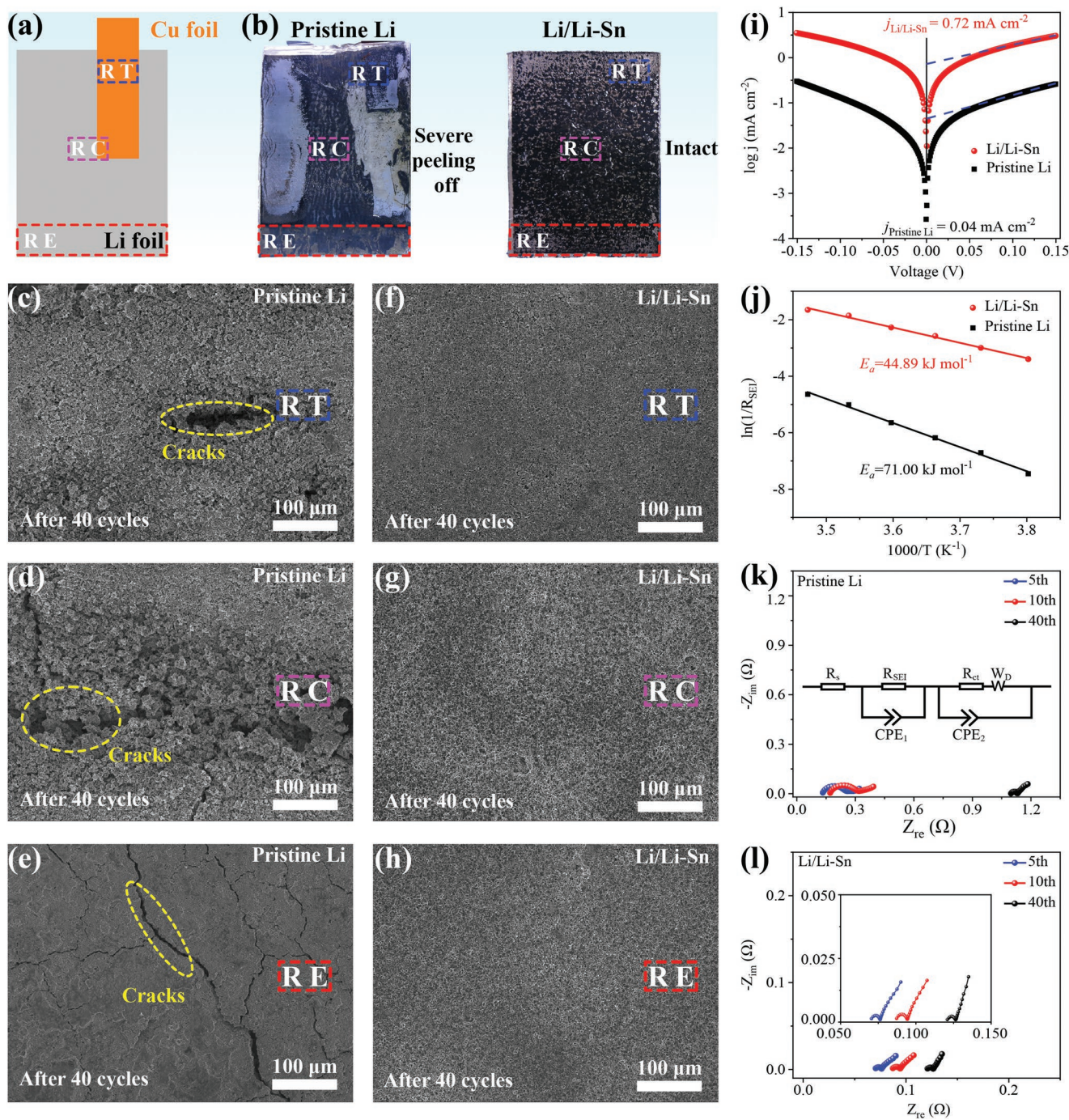


Figure 3. a) Schematic illustration of the anode construction where three selected regions were labeled with indicating boxes, including the near-tap (RT), the central (RC), and the edge (RE) regions. b) Digital photos of pristine Li (left) and Li/Li-Sn alloy composite (right) electrodes from cycled laminated pouch cells (1.2 Ah, 600 mA after 40 cycles). The corresponding top-view SEM images of c–e) pristine Li and f–h) Li/Li-Sn alloy composite electrodes in (c and f) RT, (d and g) RC, and (e and h) RE regions. i) Tafel curves of pristine Li and Li/Li-Sn symmetric cells. j) Apparent activation energy of Li^+ transfer through SEI layer for pristine Li and Li/Li-Sn alloy composite electrodes. Nyquist plots of k) pristine Li and l) Li/Li-Sn alloy composite electrodes after 5, 10, and 40 cycles. The inset shows the corresponding equivalent circuit model, where the solution, SEI layer, and charge transfer impedances are denoted as R_s , R_{SEI} , and R_{ct} .

introduction of Li-Sn alloy framework with remarkably high ion conductivity.^[10] In summary, the interfacial Li^+ transport property was significantly enhanced after replacing the pristine Li electrode with the Li/Li-Sn alloy composite electrode, which

is helpful in realizing fast and uniform Li^+ diffusion over the entire electrode to eliminate the effect of electric field difference in different regions of large-scale electrode and homogenizing Li plating/stripping reactions in practical Li metal batteries

under harsh working conditions, such as high current density and large electrode size.

To further validate the significant role of Li/Li–Sn alloy composite anode in stabilizing the electrode structure, EIS measurement was conducted on the 1.2 Ah SPAN||Li/Li–Sn and SPAN||Li pouch cells after 5, 10, and 40 cycles to compare the Li⁺ transport property and electrode stability during cycling. Nyquist plots of the two tested cells for selected cycles (5th, 10th, and 40th cycles) are shown in Figure 3k,l. The as-obtained values of each impedance component were extracted by an appropriate equivalent circuit model (inset of Figure 3k). In contrast to pristine Li anode, all the values of resistance components for the Li/Li–Sn alloy composite electrode were smaller and more stable for the selected cycles. The value of solution resistance (R_s) for the pristine Li electrode dramatically increased by 700% from the 5th cycle (0.13 Ω) to the 40th cycle (1.08 Ω), suggesting the unstable electrode due to severe side reactions between metallic Li and electrolyte (Figure S9 and Table S3, Supporting Information). By comparison, only a slight increase (from 0.07 to 0.10 Ω) was observed for the Li/Li–Sn alloy composite anode, showing the advantage of Li/Li–Sn alloy composite anode in suppressing the parasitic reactions and stabilizing the electrode. The value of the impedance of Li⁺ transfer through SEI layer (R_{SEI}) for the pristine Li electrode was increased by four times from 0.012 to 0.06 Ω for the 5th and 40th cycles (Figure S10, Supporting

Information). The fast growth of R_{SEI} during cycling could be attributed to the accumulation of by-products due to undesirable side reactions. In contrast, the Li/Li–Sn alloy composite electrode exhibited a stabilized R_{SEI} with negligible change for different tested cycles, revealing the robust interface structure. Besides, the value of the resistance of Li⁺ desolvation at electrolyte/SEI interface (R_{ct})^[22] for the Li/Li–Sn alloy composite anode was nearly an order of magnitude lower than pristine Li anode in each tested cycle (Figure S11, Supporting Information). The above results indicated that, due to the high conductivity and good stability of Li–Sn alloy framework, the Li/Li–Sn alloy composite electrode displayed reinforced Li⁺ transport property and stable electrochemical property during cycling in realistic Ah-level laminated pouch cells.

To further investigate the side reactions in Ah-level laminated pouch cells and reveal the crucial role of composite Li/Li–Sn alloy composite anode in eliminating the negative effect of electric field difference in different regions of large-scale electrode, the structures of the cycled Li and Li/Li–Sn alloy composite electrodes in the three regions (RT, RC, and RE) were investigated. As shown in Figure 4a–c, uniform and compact reaction layers with the same thickness of $\approx 50 \mu\text{m}$ were observed in all three regions of the Li/Li–Sn alloy composite anode, verifying the stable electrode structure on cycling. The small thickness of the reaction layer also indicated the significantly suppressed

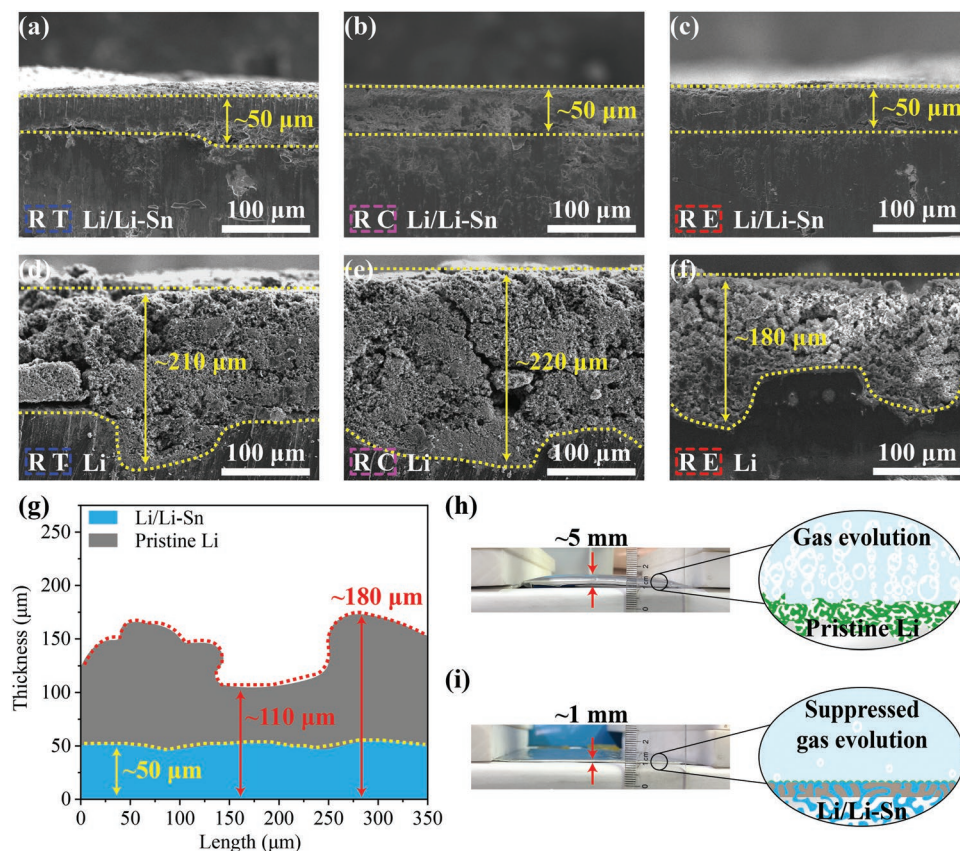


Figure 4. Cross-sectional SEM images of a–c) Li/Li–Sn alloy composite and d–f) pristine Li electrodes, obtained from the disassembled 1.2 Ah laminated pouch cells after 40 cycles in (a,d) RT, (b,e) RC, and (c,f) RE regions. g) Thickness fluctuation of reaction layers for Li/Li–Sn alloy composite and pristine Li electrodes in RE region. Optical images and corresponding schematic illustrations of gas evolution of h) SPAN||Li and i) SPAN||Li/Li–Sn laminated pouch cells after 40 cycles.

parasitic reactions of the Li/Li–Sn alloy composite electrode. In sharp contrast, pristine Li electrode displayed uneven reaction layers with a loose structure and various thicknesses in the three tested regions, which changed from 180 to 220 μm in thickness (Figure 4d–f), which was almost four times that of the Li/Li–Sn alloy composite electrode. The large thickness of the loose reaction layer indicated the much more severe side reactions of pristine Li electrode in comparison to the Li/Li–Sn alloy composite electrode in Ah-level laminated pouch cells. Taking the RE region as the example, the thickness variation of the reaction layer over the pristine Li and Li/Li–Sn alloy composite electrodes were further analyzed and illustrated in Figure 4g, according to the results of Figure 4c,f. The reaction layer of Li/Li–Sn alloy composite electrode exhibited a thin and steady thickness of $\approx 50 \mu\text{m}$ over the observed area with a width of 350 μm , while the thickness drastically varied from 110 to 180 μm for the pristine Li electrode, exhibiting a thick reaction layer with sharply fluctuant structure caused by the uneven Li plating/stripping behavior and severe corrosion. Moreover, the RT and RC regions showed a thicker and looser reaction layer than the RE region, which could be ascribed to the more inhomogeneous Li plating/stripping reactions and destructive corrosion in those areas caused by the locally magnified current densities, in agreement with the results of Figure 3c–e.

The gas evolution is accompanied by the parasitic reactions between the active material and electrolyte, which cannot be detected in coin cell configuration, and is often overlooked. In practical Ah-level laminated pouch cells, gas evolution is one main reason that leads to fast cell failure, and even causes safety hazards. We observed obvious swelling of the 1.2 Ah SPAN||Li laminated pouch cell after 40 cycles with huge volume expansion from the initial ≈ 1 to ≈ 5 mm (Figure 4h) in accordance with its severe side reactions during cycling. By comparison, the SPAN||Li/Li–Sn pouch cell remained in the initial thickness without obvious swelling in volume (Figure 4i), demonstrating suppressed gas evolution due to the use of the Li/Li–Sn alloy composite anode.

A non-destructive ultrasonic imaging technique^[23] was further employed to monitor the gassing behavior of the SPAN||Li

and SPAN||Li/Li–Sn pouch cells with a size of 8×11 cm. The gas evolution that leads to a strong reflection of ultrasonic signal would significantly increase the acoustic impedance of cells and decrease the ultrasonic wave transmittance. Therefore, the gas evaluation of pouch cells could be detected and compared, reflecting the state of health of batteries. During the measurement, high-to-low ultrasonic transmissivity was converted into a red-to-blue heat map (Figure 5), where blue represented low transmissivity, implying gas evolution. Figure 5a shows the result of ultrasonic imaging for the fresh SPAN||Li cell before cycling and its well-wetted condition was confirmed. The slight color difference in the color of the image reflected the small difference in cell structure during its fabrication, which could be ignored in the measurement. In the RT and RC regions, the initial colors started to turn blue after 20 cycles, and thus the gas generation in these two regions was confirmed (Figure 5b). This result was consistent with the severe corrosion phenomenon in these two regions observed by SEM (Figure 3c,d and Figure 4d,e), further verifying the interregional inhomogeneity between RE and other regions arising from their different local electrochemical environments. Moreover, the entire test region turned blue after 40 cycles (Figure 5c), revealing the numerous accumulated gases inside the SPAN||Li pouch cell due to the continuous side reactions during cycling. The uneven Li plating/stripping behavior for pristine Li anode caused severe side reactions, leading to fast electrolyte consumption, gas generation and performance degradation. By contrast, the result of ultrasonic imaging for SPAN||Li/Li–Sn cell exhibited no color change after 20 cycles (Figure 5e) and only slight color change after 40 cycles (Figure 5f), demonstrating the significantly suppressed gas evolution behavior. Thus, by replacing the pristine Li electrode with the Li/Li–Sn alloy composite electrode, more stable electrode structure can be realized and the undesirable parasitic reactions can be effectively hindered in practical laminated pouch cells.

The homogeneity of electrochemical reactions and structure evolution of the pristine Li and Li/Li–Sn alloy composite electrodes in pouch cells was schematically shown in Figure 6. Besides the inherent uneven electrochemical Li

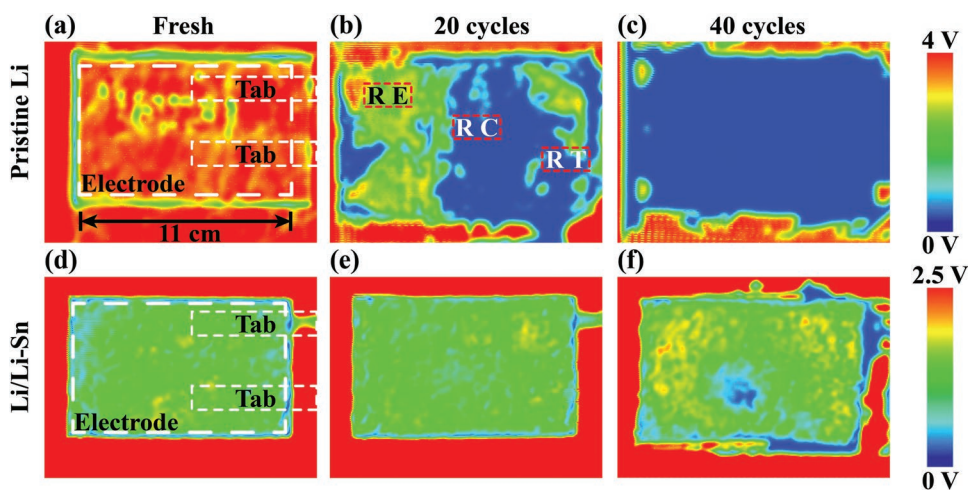


Figure 5. Ultrasonic transmission mappings of a–c) SPAN||Li and d–f) SPAN||Li/Li–Sn laminated pouch cells with large electrode size of 8×11 cm (a and d) before cycling, (b and e) after 20 cycles, and (c and f) 40 cycles at 0.5 C. The unit “V” of the color bar stands for voltage.

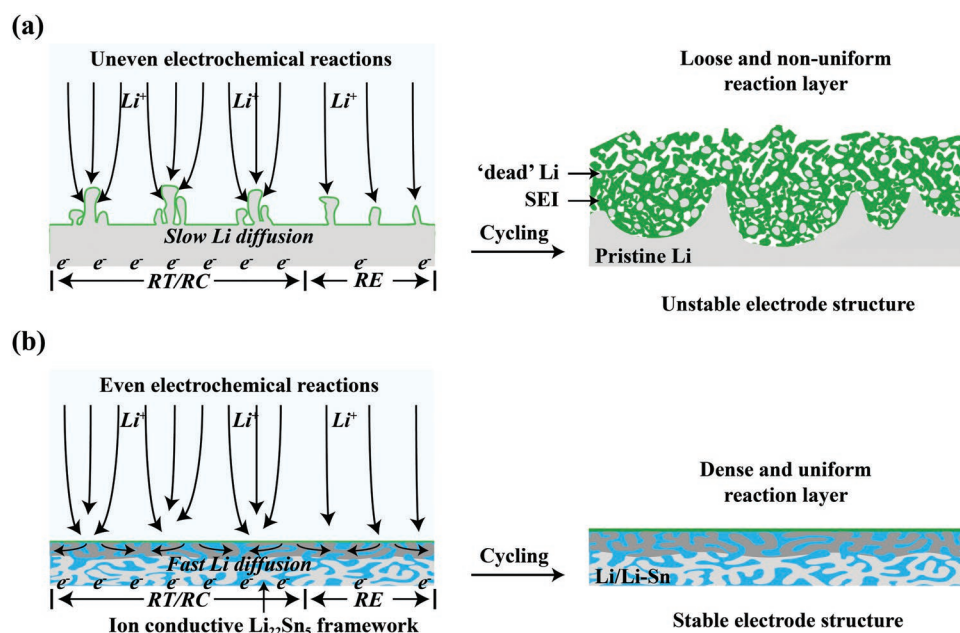


Figure 6. Schematic illustration of the proposed evolution of a) pristine Li and b) Li/Li–Sn alloy composite electrodes in laminated pouch cells during cycling. The enhanced ion transport property and robust Li–Sn alloy framework structure of Li/Li–Sn alloy composite electrode enable fast lithium diffusion and stable electrode structure, leading to extended cycle life.

plating/stripping behavior of the pristine Li electrode, the construction of practical laminated pouch cells amplified the inhomogeneity of electrochemical reactions, accelerating the battery failure. Due to the difference in electrochemical environment for different regions of large-scale electrode, the inhomogeneous current distribution over the large-scale pristine Li electrode further caused the uneven electrochemical reactions and detrimental parasitic reactions, and the resulting fast accumulation of by-products and formation of loose and non-uniform reaction layer, which was accompanied by the fast consumption of electrolyte and active Li (Figure 6a). The negative effect of inhomogeneity of electrochemical reactions in practical laminated pouch cells could be well addressed by Li/Li–Sn alloy composite electrode design due to the fast Li diffusion capability in ion conductive Li–Sn alloy pathway and stable interphase in contact with electrolyte, where electrochemical reactions take place over the entire electrode instead of electrode surface.^[10] Also, the capability of Li^+ transport could be reinforced, which helped to enable uniform Li plating/stripping behavior and suppressed the growth of Li dendrites, thus extending the battery cycle life (Figure 6b).

3. Conclusion

In summary, this work analyzed the difference in electrochemical Li plating/stripping behavior between coin cell and pouch cell, and revealed the intrinsic inhomogeneity of electrochemical reactions caused by pouch cell structure, which explained the much faster electrochemical failure of Li metal electrode in Ah-level laminated pouch cell in comparison to coin cell. Composite Li metal anode with high ion conductivity could enable stable electrochemical reactions in Ah-level laminated

pouch cells with large-scale electrodes. Compared to pristine Li anode, Li/Li–Sn alloy composite anode displayed a stable electrode structure with a dense and uniform reaction layer over the entire electrode with a size of 8×11 cm, suppressed gas evolution behavior, and enhanced cycling stability. By pairing with a high-loading SPAN cathode (3.4 mA h cm^{-2} , N/P ratio of 4.9), SPAN||Li/Li–Sn cells delivered high capacity-retention up to 87% for 100 cycles in a practical 1.2 Ah laminated pouch cell under a high current of 600 mA, far outperforming the SPAN||Li cells. This work discloses the uneven electrochemical reactions that pouch cell structure causes, and demonstrates the potential for applying the composite Li electrode design with high ion conductivity to eliminate the negative effect of inhomogeneity of electrochemical reactions caused by the pouch cell structure and prolong the lifespan of practical Li metal pouch cells, which opens a promising avenue toward the next-generation high energy density lithium metal batteries.

4. Experimental Section

All experimental details are included in the Supporting Information.

Supporting Information

Supporting Information is available from the Wiley Online Library or from the author.

Acknowledgements

Y.S. acknowledges the support from the Natural Science Foundation of China (grant no. 52272207, 52072137). This work was supported by

the Analytical and Testing Center of Huazhong University of Science and Technology (HUST). Z.W.S. acknowledges the Agency for Science, Technology and Research (Central Research Fund Award).

Conflict of Interest

The authors declare no conflict of interest.

Data Availability Statement

Research data are not shared.

Keywords

electrochemical performance, laminated pouch cells, Li metal electrodes, Li/Li–Sn alloy composite electrodes, uneven electrochemical reactions

Received: September 13, 2022

Revised: November 11, 2022

Published online:

- [1] a) V. Etacheri, R. Marom, R. Elazari, G. Salitra, D. Aurbach, *Energy Environ. Sci.* **2011**, *4*, 3243; b) P. G. Bruce, S. A. Freunberger, L. J. Hardwick, J.-M. Tarascon, *Nat. Mater.* **2012**, *11*, 19; c) J. W. Choi, D. Aurbach, *Nat. Rev. Mater.* **2016**, *1*, 16013.
- [2] a) H. Yuan, X. Ding, T. Liu, J. Nai, Y. Wang, Y. Liu, C. Liu, X. Tao, *Mater. Today* **2022**, *53*, 173; b) P. Zou, Y. Sui, H. Zhan, C. Wang, H. L. Xin, H.-M. Cheng, F. Kang, C. Yang, *Chem. Rev.* **2021**, *121*, 5986.
- [3] a) Y. Xiang, M. Tao, G. Zhong, Z. Liang, G. Zheng, X. Huang, X. Liu, Y. Jin, N. Xu, M. Armand, J.-G. Zhang, K. Xu, R. Fu, Y. Yang, *Sci. Adv.* **2021**, *7*, eabj3423; b) X. Fan, C. Wang, *Chem. Soc. Rev.* **2021**, *50*, 10486.
- [4] a) Z. Peng, X. Cao, P. Gao, H. Jia, X. Ren, S. Roy, Z. Li, Y. Zhu, W. Xie, D. Liu, Q. Li, D. Wang, W. Xu, J.-G. Zhang, *Adv. Funct. Mater.* **2020**, *30*, 2001285; b) J. Langdon, R. Sim, A. Manthiram, *ACS Energy Lett.* **2022**, *7*, 2634.
- [5] R. Weber, M. Genovese, A. J. Louli, S. Hames, C. Martin, I. G. Hill, J. R. Dahn, *Nat. Energy* **2019**, *4*, 683.
- [6] T. Li, P. Shi, R. Zhang, H. Liu, X.-B. Cheng, Q. Zhang, *Nano Res.* **2019**, *12*, 2224.
- [7] Y. Liu, X. Tao, Y. Wang, C. Jiang, C. Ma, O. Sheng, G. Lu, W. L. Xiong, *Science* **2022**, *375*, 739.
- [8] H. Chen, Y. Yang, D. T. Boyle, Y. K. Jeong, R. Xu, L. S. de Vasconcelos, Z. Huang, H. Wang, H. Wang, W. Huang, H. Li, J. Wang, H. Gu, R. Matsumoto, K. Motohashi, Y. Nakayama, K. Zhao, Y. Cui, *Nat. Energy* **2021**, *6*, 790.
- [9] P. Shi, X. Q. Zhang, X. Shen, B. Q. Li, R. Zhang, L. P. Hou, Q. Zhang, *Adv. Funct. Mater.* **2020**, *31*, 2004189.
- [10] M. Wan, S. Kang, L. Wang, H. W. Lee, G. W. Zheng, Y. Cui, Y. Sun, *Nat. Commun.* **2020**, *11*, 829.
- [11] a) S. Chen, C. Niu, H. Lee, Q. Li, L. Yu, W. Xu, J.-G. Zhang, E. J. Dufek, M. S. Whittingham, S. Meng, J. Xiao, J. Liu, *Joule* **2019**, *3*, 1094; b) J. Liu, Z. Bao, Y. Cui, E. J. Dufek, J. B. Goodenough, P. Khalifah, Q. Li, B. Y. Liaw, P. Liu, A. Manthiram, Y. S. Meng, V. R. Subramanian, M. F. Toney, V. V. Viswanathan, M. S. Whittingham, J. Xiao, W. Xu, J. Yang, X.-Q. Yang, J.-G. Zhang, *Nat. Energy* **2019**, *4*, 180.
- [12] C. Niu, D. Liu, J. A. Lochala, C. S. Anderson, X. Cao, M. E. Gross, W. Xu, J.-G. Zhang, M. S. Whittingham, J. Xiao, J. Liu, *Nat. Energy* **2021**, *6*, 723.
- [13] X.-B. Cheng, C. Yan, J.-Q. Huang, P. Li, L. Zhu, L. Zhao, Y. Zhang, W. Zhu, S.-T. Yang, Q. Zhang, *Energy Storage Mater.* **2017**, *6*, 18.
- [14] a) S. P. V. Nadimpalli, V. A. Sethuraman, D. P. Abraham, A. F. Bower, P. R. Guduru, *J. Electrochem. Soc.* **2015**, *162*, A2656; b) D. Ren, X. Feng, L. Lu, X. He, M. Ouyang, *Appl. Energy* **2019**, *250*, 323.
- [15] C. Fang, B. Lu, G. Pawar, M. Zhang, D. Cheng, S. Chen, M. Ceja, J.-M. Doux, H. Musrock, M. Cai, B. Liaw, Y. S. Meng, *Nat. Energy* **2021**, *6*, 987.
- [16] C. Niu, H. Lee, S. Chen, Q. Li, J. Du, W. Xu, J.-G. Zhang, M. S. Whittingham, J. Xiao, J. Liu, *Nat. Energy* **2019**, *4*, 551.
- [17] a) Y. Chen, M. Yue, C. Liu, H. Zhang, Y. Yu, X. Li, H. Zhang, *Adv. Funct. Mater.* **2019**, *29*, 1806752; b) Y. Hu, Y. Ren, R. Shi, J. Yu, Z. Sun, S. Guo, J. Guo, F. Yan, *ACS Appl. Mater. Interfaces* **2021**, *13*, 16289; c) X. Lin, J. Yu, M. B. Effat, G. Zhou, M. J. Robson, S. C. T. Kwok, H. Li, S. Zhan, Y. Shang, F. Ciucci, *Adv. Funct. Mater.* **2021**, *31*, 2101261.
- [18] a) L. P. Hou, N. Yao, J. Xie, P. Shi, S. Y. Sun, C. B. Jin, C. M. Chen, Q. B. Liu, B. Q. Li, X. Q. Zhang, Q. Zhang, *Angew. Chem., Int. Ed.* **2022**, *61*, e202201406; b) M. Zhao, X. Chen, X. Y. Li, B. Q. Li, J. Q. Huang, *Adv. Mater.* **2021**, *33*, 2007298.
- [19] a) X. Chen, L. Peng, L. Wang, J. Yang, Z. Hao, J. Xiang, K. Yuan, Y. Huang, B. Shan, L. Yuan, J. Xie, *Nat. Commun.* **2019**, *10*, 1021; b) Z. Wu, H. Liu, S. Yu, P. Liu, *J. Electrochem. Soc.* **2021**, *168*, 110504; c) Z. Wu, H. Liu, J. Holoubek, C. Anderson, L. Shi, H. Khemchandani, D. Lu, D. Liu, C. Niu, J. Xiao, P. Liu, *ACS Energy Lett.* **2022**, *7*, 2701.
- [20] a) L. Fu, X. Wang, L. Wang, M. Wan, Y. Li, Z. Cai, Y. Tan, G. Li, R. Zhan, Z. W. Seh, Y. Sun, *Adv. Funct. Mater.* **2021**, *31*, 2101602; b) J. Du, W. Wang, M. Wan, X. Wang, G. Li, Y. Tan, C. Li, S. Tu, Y. Sun, *Adv. Energy Mater.* **2021**, *11*, 2102259.
- [21] L. Fu, X. Wang, Z. Chen, Y. Li, E. Mao, Z. W. Seh, Y. Sun, *Carbon Energy* **2022**, *4*, 12.
- [22] Z. Wang, F. Qi, L. Yin, Y. Shi, C. Sun, B. An, H.-M. Cheng, F. Li, *Adv. Energy Mater.* **2020**, *10*, 1903843.
- [23] a) Z. Deng, Z. Huang, Y. Shen, Y. Huang, H. Ding, A. Luscombe, M. Johnson, J. E. Harlow, R. Gauthier, J. R. Dahn, *Joule* **2020**, *4*, 2017; b) J. Xiang, Y. Zhang, B. Zhang, L. Yuan, X. Liu, Z. Cheng, Y. Yang, X. Zhang, Z. Li, Y. Shen, J. Jiang, Y. Huang, *Energy Environ. Sci.* **2021**, *14*, 3510.